

# The Disappearance of the Progenitors of Supernovae 1993J and 2003gd

Justyn R. Maund,<sup>\*,1,2,3</sup> Stephen J. Smartt,<sup>4</sup>

<sup>1</sup> Dark Cosmology Centre, Niels Bohr Institute, University of Copenhagen  
Juliane Maries Vej 30, 2100 Copenhagen Ø, Denmark

<sup>2</sup> Department of Astronomy & Astrophysics, University of California, Santa Cruz, 95064, U.S.A.

<sup>3</sup> Sophie & Tycho Brahe Fellow

<sup>4</sup> Astrophysics Research Centre, School of Mathematics and Physics,  
Queens' University Belfast, Belfast, BT7 1NN, United Kingdom

\*To whom correspondence should be addressed;  
E-mail: justyn@dark-cosmology.dk.

**Using images from the Hubble Space Telescope (HST) and the Gemini Telescope we confirm the disappearance of the progenitors of two Type II supernovae (SNe), and evaluate the presence of other stars associated with them. We find that the progenitor of SN 2003gd, an M-supergiant star, is no longer observed at the SN location, and determine its intrinsic brightness using image subtraction techniques. The progenitor of SN 1993J, a K-supergiant star, is also no longer present, but its B-supergiant binary companion is still observed. The disappearance of the progenitors confirms that these two SNe were produced by Red Supergiants.**

Analysis of archival pre-explosion images has helped to identify the progenitors of type II supernovae, which are thought to result from the explosion of red supergiant stars. In most

cases the progenitors have only been confirmed to be spatially coincident with the SNe, leaving some uncertainty over their correct identification. So far only one star has been shown to have disappeared after it exploded - the star that exploded as SN 1987A in the Local Group of galaxies (1). Seven other stars have been discovered to be spatially coincident with bright, nearby type II SNe (2), but none of them have been shown to have disappeared [although recent evidence has suggested the disappearance of the progenitor of SN2005gl (3)]. Here we examine post-explosion images of the sites of two type II SNe to confirm their progenitors' identity.

SN 2003gd was discovered in the galaxy M74 and classified as a type II-plateau SN (4). The plateau in its light curve and the strong hydrogen P Cygni profiles in its spectrum indicated that it arose from a red supergiant star with a massive hydrogen envelope (5). Analysis of pre-explosion images from the Hubble Space Telescope (HST) and Gemini Telescope archives revealed a red supergiant star, with  $V = 25.8$ ,  $I = 23.3$  and an initial mass of  $8_{-2}^{+4}$  solar masses ( $M_{\odot}$ ), at the position where the SN occurred (see Fig. 1; (6, 7)). Five years after the explosion it is time to verify that this star has disappeared, hoping that the SN remnant has faded to a luminosity below that of its progenitor (as achieved for SN 1987A).

We re-imaged the site of SN 2003gd on 6 and 10 September 2008 using the multiobject spectrograph [GMOS, (8)] on the Gemini Telescope with the Sloan  $g'$ ,  $r'$  and  $i'$  filters, under excellent seeing conditions (see Table 1). Using differential astrometry, we matched previous observations of SN 2003gd, acquired with the HST Advanced Camera for Surveys High Resolution Channel (ACS HRC) (6), with our GMOS frames to locate the SN position to within  $0.031''$  (see Fig. 1). At this position there is no significant detection of a point source in the  $i'$  image, but the SN is still detected significantly at  $m_{g'}(AB) = 25.00 \pm 0.04$  and  $m_{r'}(AB) = 24.65 \pm 0.05$  (see SOM). We compared our  $i'$  image with a pre-explosion  $i'$  image taken with the GMOS instru-

ment on 14 Aug 2001, in which the progenitor candidate was detected. After aligning the two images, we scaled the flux levels and the Point-Spread Function (PSF) of the post-explosion  $i'$ -band image to match those of the pre-explosion image, using the *ISIS* image subtraction package (9, 10). We then subtracted the scaled post-explosion image from the pre-explosion frame, such that only photometrically variable objects remained (see the SOM for details of the procedure). A point source residual, consistent with a single-star PSF, is present in the pre-explosion image to within  $0.023''$  of the transformed SN position (see Fig. 1, see SOM). Ref. (6) found a large offset between the transformed SN position and the object on the pre-explosion frame ( $0.137 \pm 0.071''$ ), leading them to suggest that the object was a blend of the progenitor (Star A) and a nearby star (Star C, see Fig. 1). We find no such offset with our differential astrometric solution, such that the object on the pre-explosion frame is completely consistent with a single star located at the position of Star A. All other single non-variable stellar objects were cleanly subtracted from the pre-explosion image, with only minor residuals remaining for obviously extended features such as resolved clusters. Hence the point source visible in the subtracted frame is the  $i'$ -band flux from the progenitor which has now disappeared. There clearly is a faint, extended background feature in the post-explosion image, but this is inconsistent with a single PSF. By conducting forced photometry at the SN position and by adding artificial stars to our post-explosion  $i'$  image, and attempting to recover them using the *ISIS* package, we conservatively estimate the upper brightness limit for a single point source is  $m_i(AB) > 26.3$  at the SN location. This corresponds to a magnitude difference between the pre- and post-explosion  $i'$  images of  $\Delta m_{i'} > 2$ . The absence of an obvious point source in the post-explosion image, which is within 2 magnitudes of the detected progenitor, further confirms that the star has disappeared.

We transformed the pre-explosion  $i'$  band photometry to the Johnson system by bootstrapping the photometry with Wide Field Camera images, from the Isaac Newton Telescope, and

the M74 standard star sequence used for monitoring both SN 2003gd and SN 2002ap (11). These data imply that the progenitor star had a final Johnson  $I$  band magnitude of  $23.14 \pm 0.08$ , tightening earlier constraints (6). This is 0.2 mags brighter than previously reported, due to our determination that Star C contributed negligible  $i'$  flux.

Using the HSTphot package (S1), we analyzed pre-explosion HST WFPC2 images taken with the  $F606W$  filter, which is close to the V-band filter. We used the  $I$ -band magnitude determined above to solve the color-transformation equations that convert the  $F606W$  instrumental magnitude to the Johnson system, and found that the progenitor has a Johnson V magnitude of  $25.72 \pm 0.09$ . Correcting for a reddening of  $E(B - V) = 0.14 \pm 0.06$ , which was determined from photometry of SN 2003gd (5), implies an intrinsic color of  $(V - I)_0 = 2.41 \pm 0.14$ . This is consistent with the progenitor being a M0-M2 Red Supergiant star (13), but disfavors warmer K-supergiant stars. Applying the appropriate bolometric correction for this range of allowed red supergiants, and correcting for a distance of  $9.3 \pm 1.8$  Mpc to M74 (5), yields a luminosity of  $\log(L/L_\odot) = 4.29 \pm 0.2$  with an effective temperature of  $\log T_{eff} = 3.54 \pm 0.02$ . Comparison with the end-points of stellar evolution models shows that this luminosity and temperature region of the Hertzsprung-Russell diagram constrains the progenitor to have had initial mass of  $7_{-1}^{+6} M_\odot$  (2).

At the epoch of 6 September 2008 (approximately +2000 days after explosion), the SN is still visible in the wavelength range corresponding to the F622W and Sloan  $r'$  filters (See Table S7). This is due to the presence of significant  $H\alpha$  emission in the band-passes of these filters, typical of Type II SNe at late times (5, 14). The fact that the SN is bright in the late-time F622W observations precludes the use of image subtraction techniques to determine the true progenitor brightness in the pre-explosion WFPC2 F606W image. We need to wait longer until the  $H\alpha$

flux fades well below the magnitude of the progenitor star detected in the F606W filter.

One could argue that the star identified as the progenitor was a neighbouring star that is now obscured by dust formation in the foreground SN remnant. However the internal extinction in the SN 2003gd remnant, due to newly formed dust was estimated to be  $A_R < 1.48$  (15) or  $A_V < 1.22$  (16) at 678 days. Using this as the maximum value of the extinction across the SN remnant at the epoch of our GMOS images (assuming no further dust formation), this amount of extinction is insufficient to cause  $\Delta m_V$  measured by us. This implies that the object we have identified as the progenitor is not simply obscured by dust in the intervening SN remnant and has actually disappeared.

The progenitor of the Hydrogen-bearing (Type IIb) SN 1993J was identified as a K-supergiant star, with excess flux in the ultra-violet, possibly because of a binary companion or nearby stars (17). The model for this binary system was of a  $15M_\odot$  progenitor star, with a binary companion of slightly lower mass (18, 19, 20). Because the progenitor star evolved faster, it underwent mass transfer onto the binary companion, which removed a substantial amount of its Hydrogen envelope, causing a shift to the bluer K-spectral type [rather than the canonical M spectral type (2)]. The binary companion grew to  $22M_\odot$ , and became the source of the excess ultra-violet flux. A later study, using high-resolution HST images, found that some of the UV excess could be explained by nearby previously unresolved stars, but that a UV excess still remained unaccounted for (21). The binary progenitor scenario was confirmed, when spectral features of a massive blue supergiant were detected in late-time spectroscopy (22).

The site of SN 1993J was imaged several times over the 2-13 years after explosion with the HST WFPC2, ACS HRC and Wide-field Channels (WFC) (see SOM for full list of dates). By

the epoch of the 2004 observation, the red portion of the SN spectral energy distribution (SED) had faded below the level of the SED of the binary progenitor system (Fig. 2, see SOM), ruling out the continued presence of the K-supergiant star and, hence, confirming it as the progenitor of SN 1993J. At the current rate of decay of the SN SED, the U and B-band fluxes will have reached the level of the proposed B-supergiant component by 2012, at which stage it will be possible to directly measure the properties of the remaining companion star.

These results provide observational proof that red supergiant stars are the progenitors of type II SNe, through the disappearance of the previously identified candidate stars of two SNe. Our best estimate for the mass of the progenitor of the Type IIP SN 2003gd is  $7M_{\odot}$  which is at the lower end of the mass range considered theoretically possible to produce core-collapse events. While the uncertainties ( $7_{-1}^{+6}M_{\odot}$ ) would comfortably allow a large mass for this object, it is interesting that five progenitors of Type IIP SNe are found with best estimates at  $9M_{\odot}$  or below (2). This limit is predicted by stellar and SN evolution models (23) and is consistent with the upper initial mass limit observed for white dwarfs (24). The confirmation of the disappearance of the K-type progenitor star of SN1993J is further evidence that the binary model previously suggested is valid. It demonstrates the importance of binary interactions for the production of Hydrogen poor SNe (25).

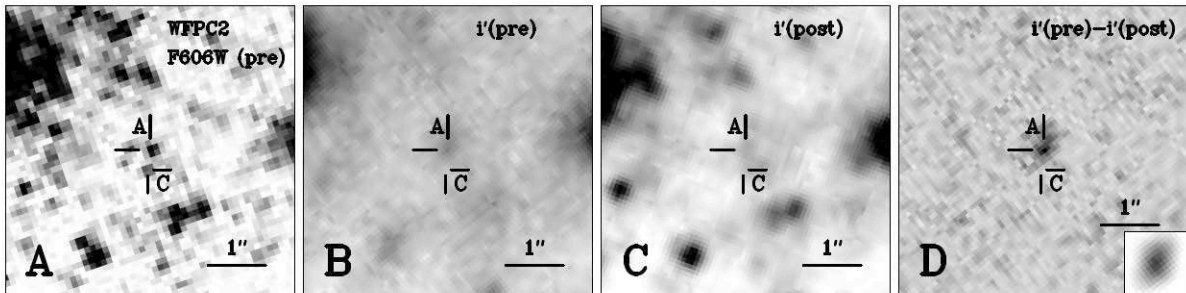


Figure 1: Pre- and post-explosion images of the site of SN 2003gd taken with the HST WFC2 and Gemini GMOS instruments (see Table 1 for details). **(A)** Pre-explosion WFC2 F606W image, with the previously identified progenitor object marked as Star A, and a nearby star labelled Star C. **(B)** Pre-explosion Gemini GMOS  $i'$  band image, with spatial resolution  $0.57''$ , in which the progenitor is detected. **(C)** Post-explosion Gemini GMOS  $i'$  band image where a single point source is not detected at the transformed position of SN 2003gd, with a limit on any remaining SN flux of  $m_{i'}(AB) > 26.3$ . The image has a spatial resolution of  $0.36''$  and no point source is detected at the position of Star C, suggesting a negligible contribution in the  $i'$ -band from that star. **(D)** Pre-explosion image with the flux/PSF-scaled post-explosion image subtracted. The residual object at the position of SN 2003gd is the progenitor, with any contaminating flux from nearby stars subtracted. The object at the SN location, marked as Star A, is consistent with single-star PSF ( $\chi^2 = 0.9$ ) and has a Johnson-I magnitude  $23.14 \pm 0.08$  ( $m_{i'}(AB) = 24.25 \pm 0.04$ ). In the bottom right hand corner a model single star PSF is shown. It was determined by *ISIS* and is consistent with the source detected in this subtraction image.

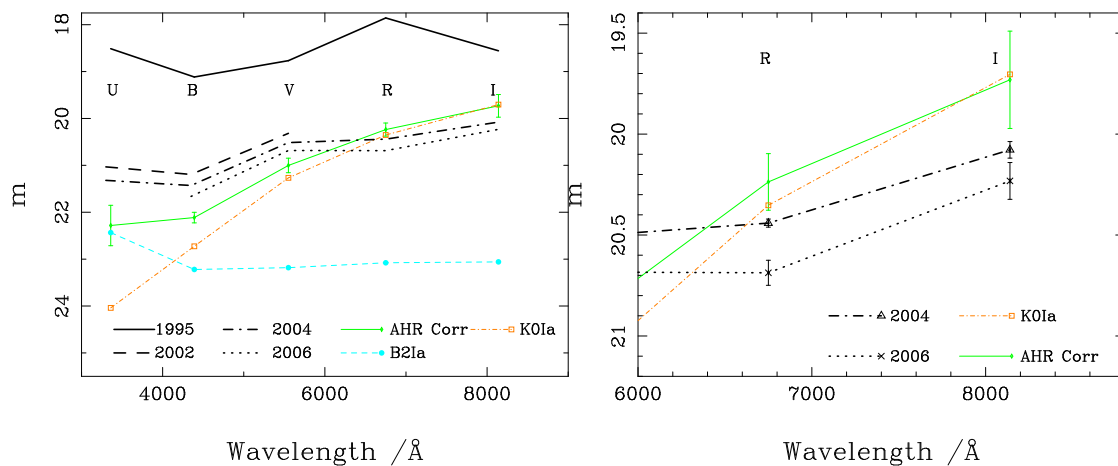


Figure 2: The Spectral Energy Distribution of the progenitor binary system of SN 1993J. The SED (AHR Corr) has been corrected for the excess flux contribution from four nearby stars, unresolved in the low-resolution ground-based pre-explosion imaging, for comparison with photometry of high-resolution HST imaging in which the SN is resolved. **(Left)** Overlaid SN 1993J SEDs, measured with HST WFPC2, ACS/HRC and ACS/WFC, at 31 Jan 1995, 28 May 2002, 15 Jul 2004 and 1 and 3 Nov 2006. The B and K supergiant components are the result of a  $\chi^2$  fit to the excess corrected pre-explosion photometry (22, 26). **(Right)** A zoom in on the  $R_C$  and  $I_C$  photometric points. Errors on the 2004 and 2006 photometry are calculated from PSF photometry of SN 1993J.

Table 1: Pre- and post-explosion observations of the site of SN 2003gd. (\*pixel scale)

Telescope/ Instrument	Date	Program	Filter	Exposure Time(s)	Seeing (")
Gemini GMOS	14 Aug 2001	GN-2001B-SV-102	$i'$	480	0.57
HST/WFPC2	25/28 Aug 2002	GO-9676	F606W	2100	0.1*
HST/ACS/HRC	01 Aug 2003	GO-9733	F814W	1350	0.025*
Gemini GMOS	10 Sep 2008	GN-2008B-Q-67	$g'$	4050	0.53
Gemini GMOS	06 Sep 2008	GN-2008B-Q-67	$r'$	1590	0.42
Gemini GMOS	06 Sep 2008	GN-2008B-Q-67	$i'$	3180	0.36

## References and Notes

1. R. Gilmozzi, *et al.*, *Nature* **328**, 318 (1987).
2. S. J. Smartt, J. J. Eldridge, R. M. Crockett, J. R. Maund, *ArXiv*, astro-ph/0809.0403 (2008).
3. A. Gal-Yam, D. Leonard, *Nature*, DOI 10.1038/nature07934 (2009).
4. R. Evans, R. H. McNaught, *IAU Circ.* **8150**, 2 (2003).
5. M. A. Hendry, *et al.*, *MNRAS* **359**, 906 (2005).
6. S. J. Smartt, *et al.*, *Science* **303**, 499 (2004).
7. S. D. Van Dyk, W. Li, A. V. Filippenko, *PASP* **115**, 1289 (2003).
8. I. M. Hook, *et al.*, *PASP* **116**, 425 (2004).
9. C. Alard, R. H. Lupton, *ApJ* **503**, 325 (1998).
10. C. Alard, *A&AS* **144**, 363 (2000).
11. A. Henden, *GRB Coordinates Network* **1242**, 1 (2002).
12. A. E. Dolphin, *PASP* **112**, 1383 (2000).
13. J. H. Elias, J. A. Frogel, R. M. Humphreys, *ApJS* **57**, 91 (1985).
14. A. Pastorello, *et al.*, *ArXiv*, astro-ph/0901.2075 (2009).
15. B. E. K. Sugerman, *et al.*, *Science* **313**, 196 (2006).
16. J. A. Cardelli, G. C. Clayton, J. S. Mathis, *ApJ* **345**, 245 (1989).
17. G. Aldering, R. M. Humphreys, M. Richmond, *AJ* **107**, 662 (1994).

18. K. Nomoto, *et al.*, *Nature* **364**, 507 (1993).
19. P. Podsiadlowski, J. J. L. Hsu, P. C. Joss, R. R. Ross, *Nature* **364**, 509 (1993).
20. S. E. Woosley, R. G. Eastman, T. A. Weaver, P. A. Pinto, *ApJ* **429**, 300 (1994).
21. S. D. Van Dyk, *et al.*, *PASP* **114**, 1322 (2002).
22. J. R. Maund, S. J. Smartt, R. P. Kudritzki, P. Podsiadlowski, G. F. Gilmore, *Nature* **427**, 129 (2004).
23. J. J. Eldridge, C. A. Tout, *MNRAS* **353**, 87 (2004).
24. K. A. Williams, M. Bolte, D. Koester, *ArXiv*, astro-ph/0811.1577 (2008).
25. P. Podsiadlowski, *et al.*, *ApJ* **612**, 1044 (2004).
26. J. R. Maund, The Observed Nature of the Progenitors of Core-collapse Supernovae, Ph.D. thesis, Institute of Astronomy, Cambridge (2005), <http://www.dark-cosmology.dk/~justyn/research/>.

27. The authors thank C. Alard for discussion about the *ISIS* code and Joanna Fabbri for discussion concerning dust formation in the remnant of SN 2003gd. The research of JRM is funded through the Sophie & Tycho Brahe Fellowship. The Dark Cosmology Centre is supported by the DNRF. This work, conducted as part of the award "Understanding the lives of massive stars from birth to supernovae" made under the European Heads of Research Councils and European Science Foundation EURYI Awards scheme, was supported by funds from the Participating Organisations of EURYI and the EC Sixth Framework Programme. Based on observations made with the NASA/ESA Hubble Space Telescope, obtained from the Data

Archive at the Space Telescope Science Institute, which is operated by the Association of Universities for Research in Astronomy, Inc., under NASA contract NAS 5-26555. These observations are associated with programs 6139, 9353, 9676, 9733, 10204, 10250, 10272, 10584, 10877, and 11229. Based on observations obtained at the Gemini Observatory, which is operated by the Association of Universities for Research in Astronomy, Inc., under a cooperative agreement with the NSF on behalf of the Gemini partnership: the National Science Foundation (United States), the Science and Technology Facilities Council (United Kingdom), the National Research Council (Canada), CONICYT (Chile), the Australian Research Council (Australia), Ministério da Ciência e Tecnologia (Brazil) and SECYT (Argentina). Gemini data acquired for programs GN-2001B-SV-102 and GN-2008B-Q-67.

# Supporting Online Material: The Disappearance of the Progenitors of Supernovae 1993J and 2003gd

## S1 Observations

The observations used in this study are listed in Tables S1, S2 for SN 1993J and Tables S3, S4, S5 and S6 for SN 2003gd. Due to space constraints, in the main body of the paper only the most appropriate observations were explicitly discussed. All the observations presented in these tables were also reduced, analysed and considered as part of the broader context of the study, and corroborated the results presented here.

The HST data were retrieved from the Space Telescope Science Institute Archive<sup>1</sup>. These data were processed by the on-the-fly-recalibration pipeline, being processed with the most up-to-date calibration frames available for the WFPC2, ACS/HRC and ACS/WFC instruments, and were retrieved in a form on which analysis could be directly conducted.

The Gemini-North GMOS data were retrieved from the Gemini Science Archive<sup>2</sup>, and were reduced with master bias and flatfield calibration frames acquired at the same epochs. The individual observations were combined using the IRAF<sup>3</sup> `gemini` package `imcoadd` task to produce combined master science frames, on which photometry could be conducted. As a dithering pattern had been employed, the coaddition of the subimages for each filter filled in any gaps between the detectors as well as move the location of any hot pixels relative to observed stars. The 2008 observations were conducted under photometric conditions, for which photometric zeropoints (for the Sloan AB magnitude system) were calculated in the standard way<sup>4</sup>.

---

<sup>1</sup><http://archive.stsci.edu/hst>

<sup>2</sup><http://archive.gemini.edu/>

<sup>3</sup>IRAF is distributed by the National Optical Astronomy Observatory, which is operated by the Association of Universities for Research in Astronomy (AURA) under cooperative agreement with the National Science Foundation.

<sup>4</sup><http://www.gemini.edu/sciops/instruments/gmos/calibration/photometric-stds>

Table S1: Late-time HST ACS observations of the site of SN 1993J.

Date (JD +2 450 000)	Dataset	Filter	Exp Time (secs)	
2002 May 28 <sup>1</sup> (2422.81)	J8DT07010	F250W	2100	HRC
	J8DT07020	F330W	1200	HRC
	J8DT07030	F435W	1000	HRC
	J8DT07040	F555W	1120	HRC
2004 Jul 15 <sup>2</sup> (3203.40)	J8ZO02010	F330W	2400	HRC
	J8ZO02040	F435W	1548	HRC
	J8ZO02020	F555W	1200	HRC
	J8ZO02030	F625W	1200	HRC
	J8ZO02050	F814W	1739	HRC
2004 Sep 15 <sup>3</sup> (3262.82)	J90L08010	F814W	1650	WFC
2005 Jan 11 <sup>2</sup> (3382.38)	J8ZO03010	F625W	1200	HRC
	J8ZO03020	F814W	1404	HRC
2006 Sep 08 <sup>4</sup> (3987.42)	J9EL14010	F435W	1200	WFC
	J9EL14020	F606W	1200	WFC
2006 Nov 1 <sup>5</sup> (4040.78)	J9NW02010	F555W	480	HRC
	J9NW02020	F814W	720	HRC
2006 Nov 3 <sup>5</sup> (4042.77)	J9NW01010	F435W	840	HRC
	J9NW01020	F625W	360	HRC

<sup>1</sup> Program 9353 (P.I. S.J. Smartt)

<sup>2</sup> Program 10204 (P.I. B.E. Sugerman)

<sup>3</sup> Program 10250 (P.I. J. Huchra)

<sup>4</sup> Program 10584 (P.I. A. Zezas)

<sup>5</sup> Program 10877 (P.I. W. Li)

Table S2: Late-time HST WFPC2 observations of the site of SN 1993J.

Date (JD +2 450 000)	Dataset	Filter	Exp Time (secs)
1995 Jan 31 <sup>1</sup> (-251.06)	U2MH0101T	F255W	2400
	U2MH0105T	F336W	1160
	U2MH0108T	F439W	1200
	U2MH010BT	F555W	900
	U2MH010DT	F675W	900
	U2MH010FT	F814W	900
2001 Jun 4 <sup>2</sup> (2064.69)	U6EH0101R	F555W	2000
	U6EH0105R	F450W	2000
	U6EH0109R	F814W	2000
2004 Sep 25 <sup>3</sup> (3273.66)	U8ZO0101M	F675W	1200
	U8ZO0102M	F555W	1100

<sup>1</sup> Program 6139 (P.I. R. Kirshner)

<sup>2</sup> Program 9073 (P.I. J. Bregman )

<sup>3</sup> Program 10204 (P.I. B. Sugerman)

Table S3: HST ACS observations of the site of SN 2003gd

Date (JD +2 450 000)	Dataset	Filter	Exp Time (secs)	
2003 Aug 01 <sup>1</sup> (2700.93)	J8NV01011	F435W	2500	HRC
	J8NV01031	F555W	1100	HRC
	J8NV01051	F814W	1350	HRC
2004 Dec 08 <sup>2</sup> (3347.93)	J8Z447011	F435W	840	HRC
	J8Z447021	F625W	360	HRC

<sup>1</sup> Program 9733 (P.I. S.J. Smartt)

<sup>2</sup> Program 10272 (P.I. A.V. Filippenko)

Table S4: HST WFPC2 observations of the site of SN 2003gd.

Date (JD +2 450 000)	Dataset	Filter	Exp Time (secs)
2002 Aug 28 <sup>1</sup> (2514.98)	U8IXCY01M	F606W	2100
2007 Jun 21 <sup>2</sup> (4273.26)	U9NW0301M	F450W	800
	U9NW0303M	F675W	360
2007 Aug 11 <sup>3</sup> (4323.61)	UA2P0501M	F622W	1600
	UA2P0505M	F814W	1600

<sup>1</sup> Program 9676 (P.I. J. Rhoads)

<sup>2</sup> Program 10877 (P.I. W. Li)

<sup>3</sup> Program 11229 (P.I. M. Meixner)

Table S5: Gemini GMOS-N observations of the site of SN 2003gd.

Date (JD +2 450 000)	Dataset	Filter	Exp Time (secs)
2001 Aug 14 <sup>1</sup> (2136.07)	1-001	r'	4 × 120
	1-005	i'	4 × 120
	1-009	g'	4 × 120
2008 Sep 06 <sup>2</sup> (4716.12)	2-002	r'	3 × 530
	3-001	i'	6 × 530
2008 Sep 10 <sup>2</sup> (4720.12)	1-001	g'	5 × 810

<sup>1</sup> Program GN-2001B-SV-102 (P.I. Gemini Staff)

<sup>2</sup> Program GN-2008B-Q-67 (P.I. J.R. Maund)

Table S6: INT WFC observations of the site of SN 2003gd.

Date (JD +2 450 000)	Dataset	Filter	Exp Time (secs)
2001 Jul 24 <sup>1</sup> (2114.71)	r268285	V	10
	r268286	V	120
	r268287	B	120
	r268289	I	120

<sup>1</sup> Observer E.P.J. van den Heuvel

Fully reduced observations of M74 using the Isaac Newton Telescope Wide field Camera, with the Harris *BVI* filters, were retrieved from the Cambridge Astronomical Survey Unit archive <sup>5</sup>.

## S2 Photometry

### S2.1 HST data

Photometry of the HST WFPC2 data was conducted using the `HSTPHOT` package (*S1*)<sup>6</sup>, which provides corrections for aperture size and charge transfer efficiency, and includes transformations for photometry from the WFPC2 magnitude system to the standard Johnson-Cousins system. In addition, in parallel, our own photometry was conducted using the `daophot` package (*S2*) in IRAF. Corrections for the charge transfer efficiency were adopted from (*S3*) and aperture corrections were taken from (*S4*). The results from this parallel analysis were identical to those provided by `HSTPHOT`.

HST ACS photometry was conducted using our own scripts (a modified version of `daophot`, which uses pre-calculated TinyTim<sup>7</sup> PSFs) and the `DOLPHOT` program <sup>8</sup>. Both of these codes provide similar corrections and transformations for the ACS system, as `HSTPHOT` does for the WFPC2 instrument. `DOLPHOT` conducts photometry of cosmic-ray rejected, distorted, combined “*crj*” images and individual distorted “*flt*” images. Our script measures photometry using the distortion corrected drizzled “*drz*” images, with the sky background unsubtracted during the drizzling process. Importantly, the photometry using the different images and different codes generally agreed with each other to within the photometric errors, but for consistency we report

---

<sup>5</sup><http://archive.ast.cam.ac.uk>

<sup>6</sup><http://purcell.as.arizona.edu/hstphot/>

<sup>7</sup><http://www.stsci.edu/software/tinytim/tinytim.html>

<sup>8</sup><http://purcell.as.arizona.edu/dolphot/>

the magnitudes reported by the DOLPHOT package.

## S2.2 Gemini Data

Photometry of the Gemini GMOS data was conducted in the standard fashion using `daophot`. Aperture corrections were determined for each of the images using bright isolated stars present in the field. PSF models were constructed for each of the images, and photometry was conducted by fitting PSFs to stars. The observations were flux calibrated using observations of the standard fields SA110-361 and SA95-100, for the nights of 06 Sep 2008 and 10 Sep 2008 respectively. Zeropoints were derived in the standard manner (S5):  $m_{g'} = 27.852 \pm 0.021$ ,  $m_{r'} = 28.229 \pm 0.037$  and  $m_{i'} = 28.215 \pm 0.023$ .

In parallel the  $g'r'i'$  magnitudes were transformed to the standard Johnson-Cousins system, by bootstrapping the photometry via INT WFC Harris BVI observations and the Henden Johnson-Cousins standard star sequence (11). The correction from Cousins I to Johnson I magnitudes, with a quadratic dependence on  $V-I$  color, was computed using the IRAF STSDAS `synphot` package and spectra from the Bruzual-Persson-Gunn-Stryker Spectrophotometry Atlas.

To test for consistency between our bootstrapped photometry and the absolute photometry derived from our zeropoints, we determined a relationship between  $i'(AB) - I_c(\text{Vega})$  and  $V - I$  using `synphot`. This yielded a correction of  $i' - I_c = +0.7$  at  $V - I = 2.5$  which is consistent with the  $I_c$  and  $i'(AB)$  magnitudes determined for progenitor of SN 2003gd using the two separate calibrations.

## S3 SN 2003gd Images

A montage of images of the site of SN 2003gd is presented as Fig. S3. Broad band photometry of SN 2003gd at multiple late-time epochs is presented as Table S7

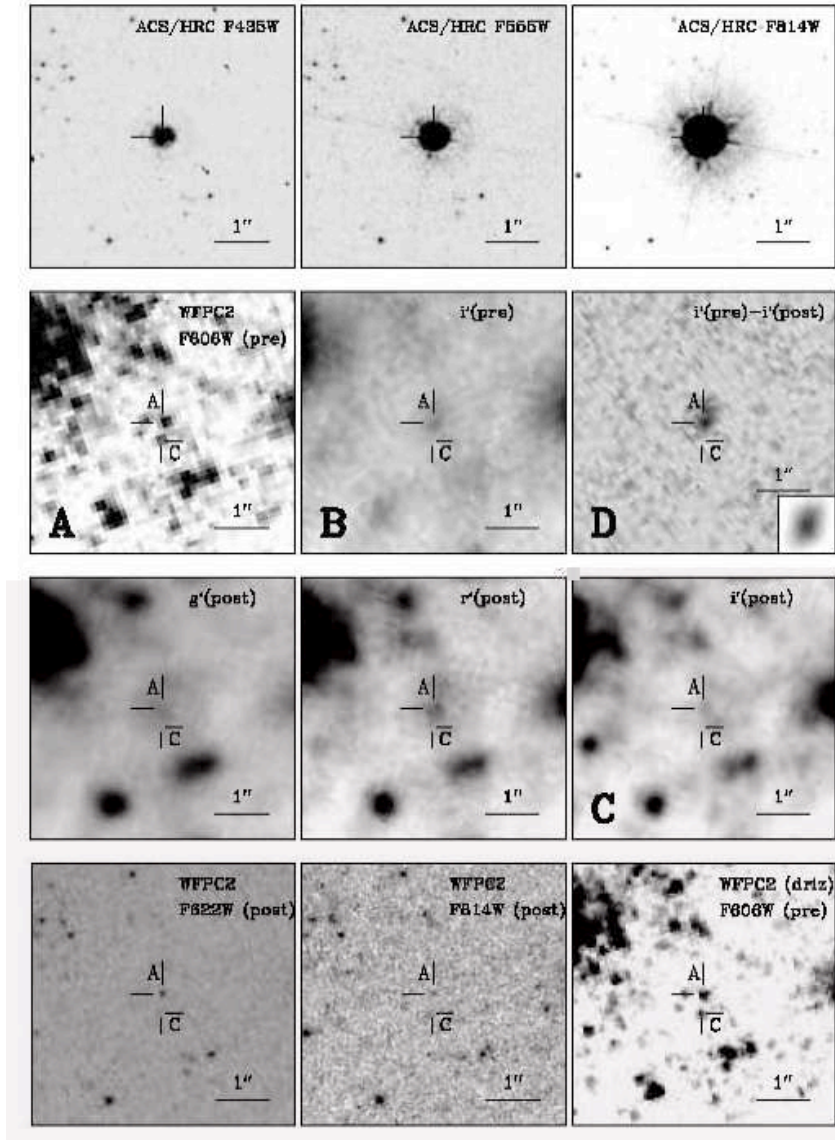


Figure S3: The site of SN 2003gd: **(First Row, l to r)** Post-explosion ACS HRC/F435W, ACS/HRC F555W and ACS/HRC F814W images (2003 Aug 01). **(Second Row, l to r)** Pre-explosion WFPC2/WF2 F606W image (2002 Aug 28), with the progenitor indicated as star A, pre-explosion Gemini GMOS  $i'$  image (2001 Aug 14), and the *ISIS* subtraction image  $i'$ (pre)- $i'$ (post). **(Third Row, l to r)** Post-explosion Gemini GMOS  $g'$ ,  $r'$  and  $i'$  images (2008 Sep 10 and 2008 Sep 06). **(Fourth Row, l to r)**, Post-explosion WFPC2/PC F622W and F814W images (2007 Aug 11) and dithered, drizzled pre-explosion F606W image with a pixel scale of 0.05". The positions of Stars A and C, as identified by Smartt et al., (6), are indicated by the cross-hairs.

Table S7: HST and Gemini photometry of SN 2003gd

Date	B	V	R	I
2003 Aug 01	19.211 (0.002)	17.480 (0.001)	...	15.869 (0.001)
2004 Dec 08	24.044 (0.037)	...	23.152 (0.041)	...
2007 June 21	25.006 (0.166)	...	24.103 (0.162)	...
2007 Aug 11*	...	...	24.445 (0.064)	25.270 (0.275)
2008 Sep 06/10 <sup>†</sup>	...	24.997 (0.042)	24.651 (0.052)	> 26.3 <sup>‡</sup>

\* Observed Vega-magnitudes for the F622W(R) and F814W(I) filters in the WFPC2 photometric system.

<sup>†</sup> AB magnitudes in the Sloan  $u'g'r'i'z'$  photometric system.

<sup>‡</sup> Assuming  $V - I = 2$  this corresponds to  $I_J = 25.2$ .

## S4 Image Subtraction

Image subtraction, and the photometry of the resulting clean images, of the SN 2003gd Gemini images was principally conducted using the *ISIS* optimized image subtraction software (9, 10)<sup>9</sup>. As the 2008 post-explosion Gemini GMOS *i'* image was acquired under better seeing conditions than the pre-explosion *i'* observation of 2001, the 2008 image was aligned with the pre-explosion observation using the *geomap* and *geotran* tasks in IRAF. Any degradation in the seeing in the resulting transformed post-explosion image was negligible compared to the much larger seeing of the pre-explosion image. The images used with the *ISIS* package were smaller  $900 \times 900$  stamps extracted from the larger observed images. The large area of these stamp images meant there were sufficient single stars, over a range of brightness, to enable the construction of a good PSF model. The transformed post-explosion image was used as the reference frame for subtraction from the pre-explosion frame using *ISIS*. *ISIS* automatically matches the PSF of the reference image to the input images, as well as appropriately scaling the flux of objects and the background. *ISIS* produces subtraction images and photometry for variable objects with different flux levels in the reference and input images. Single stellar objects, confirmed as singular on the post-explosion frame, were cleanly subtracted on the subtraction image, whereas large extended objects left minor residuals.

The photometry of *ISIS* provides a measure of the flux, in counts, of any variable objects at each epoch, along with a similar measure of flux for reference objects in the field which were not variable between the two frames. Photometry of the progenitor used the flux level of the progenitor object, reported in counts by *ISIS*, relative to the flux of these standard stars, which was converted to a magnitude using comparable *daophot* photometry of the reference stars on the post-explosion frame and the standard formula relating magnitudes and relative flux.

As *ISIS* automatically handles a large number of the details involved in image subtraction, and

---

<sup>9</sup><http://www2.iap.fr/users/alard/package.html>

is sometimes considered a “black box”, a comparable analysis was conducted in parallel using the IRAF tasks *linmatch* and *psfmatch*, which scale the flux between two aligned images and produces a convolution kernel to match the PSF of one image to another, respectively. Importantly, having run these tasks and subtracted the convoluted post-explosion image from the pre-explosion image an identical result to the *ISIS* analysis was achieved.

The quality of the PSF and the subtraction process can be estimated by studying the residual degree of flux in the self-subtracted image ( $i'(\text{post}) - i'(\text{post})$ ) after convolution and scaling. At the SN location, the residual flux is consistent with a null residual  $[(0.7 \pm 44) \times 10^{-3}]$ . The self-subtracted image is shown as Fig. S4.

The background at the SN location in the post-explosion  $i'$ -band image is particularly complex (see Fig. S3). Application of the *daophot allstar* routine, with a PSF determined from the image, does not provided a satisfactory single star solution (for either the sharpness or  $\chi^2$  parameters -  $\chi^2 = 4$ ). Synthetic artificial stars, of known magnitude, were inserted into the post-explosion frame at the SN position, using the *daophot* task *addstar*, and the *ISIS* package was used to recover them. A star of magnitude 26.5 was recovered at an 84% confidence level using *ISIS*; which we use as an estimate of the detection threshold at the SN location, on top of the complicated background structure (as *ISIS* only provides a measure of the flux difference between two images). We cannot exclude, however, the possibility that there is still some SN flux that is contributing to the detected complex background feature. In this case, therefore, a more conservative estimate was made using forced photometry at the SN position, using *daophot allstar*. We estimate an upper limit for the SN+background of 26.3, which we adopt as a conservative upper limit on the SN flux.

The likelihood of a unrelated variable object being located at the SN location was calculated in a simple fashion. The density of objects, per square pixel, was estimated using all detected variables on the  $900 \times 900$ px area. A more thorough treatment, using “association probabil-

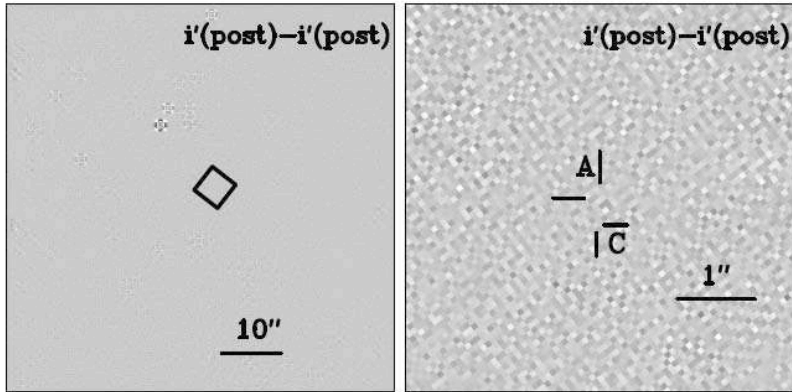


Figure S4: Self-subtracted post-explosion  $i'$  images. **(Left)**  $900 \times 900$ px frame used in the ISIS package. The black square indicates the area of the frame in which the SN is located (see next panel). Minor residuals are associated with extended objects. **(Right)** The area of the self-subtracted frame containing the SN location. The area covered by the panel corresponds exactly to the panels presented in Fig. S3.

ity analysis”, requires appropriate handling of clustering. We note that a number of identified variables occur in dense stellar regions, extended sources or moving objects, which also leave large residuals in the  $i'(post) - i'(post)$  image. The measured density is, therefore, an upper limit on the density of true variable objects, but does not include the effects of “clustering” of sources in the vicinity of the SN location (although we note that, in the case of SN 2003gd, neighbouring stars are resolved and the residual in the subtraction frame does not have the characteristic dipole signature of a moving object). The number of variable objects randomly expected within the astrometric error circle (see below) is 0.00001, suggesting the likelihood of random coincidence to be low.

## S5 Differential Astrometry

The position of the progenitor object of SN 2003gd, on each of the pre-explosion frames, was determined using differential astrometry. The position of SN 2003gd was determined from the ACS/HRC F814W observation at 01 Aug 2003. Transformations between this image and the

pre-explosion images were calculated using common stars in the images, and the IRAF task *geomap*. *geomap* also provides an estimate of the r.m.s. uncertainty associated with the transformation. The SN position from the post-explosion image was transformed to the coordinates of the pre-explosion images using the IRAF task *geoxytran*. *ISIS* provides the position of the residual on the subtraction image. The difference between the transformed position and the *ISIS* position was 0.023", whereas the uncertainty on the transformation was 0.031". Importantly, for the analysis presented here, the spatial coincidence is a secondary concern, since the identity of the progenitor has been confirmed by its absence in the post-explosion image.

## **S6 Excess flux correction for ground based imaging of the progenitor of SN 1993J**

The site of SN 1993J at 01 Nov 2006 and 03 Nov 2006, in the F814W and F625W filters respectively, is shown as Fig. S5. As the pre-explosion imaging of the progenitor (17) was ground-based, poor seeing (relative to HST observations) led to a number of bright nearby stars being unresolved and, hence, contributing flux to the measured progenitor photometry. Following previous work (21, 22), the excess flux contribution was determined by using a Gaussian-weighting scheme (where the flux contribution to the photometry of the progenitor binary is the total stellar flux for each star scaled by a factor dependent on the distance of the star from SN 1993J and the seeing, for each filter, of the pre-explosion observations). For a general filter  $X$ , the excess flux contribution to the progenitor binary photometry was calculated as:

$$F_X = \sum_{i=A..D} F_{X,i} e^{-r_i^2/4\sigma_X^2} \quad (1)$$

where  $r$  is the distance in arcseconds of the  $i$ th star from SN 1993J (measured from the ACS/HRC images) and  $\sigma_X$  is the seeing, for each filter, in the original pre-explosion imaging (17, 21). The pre-explosion photometry is in the Landolt system, and our ACS photometry has been converted

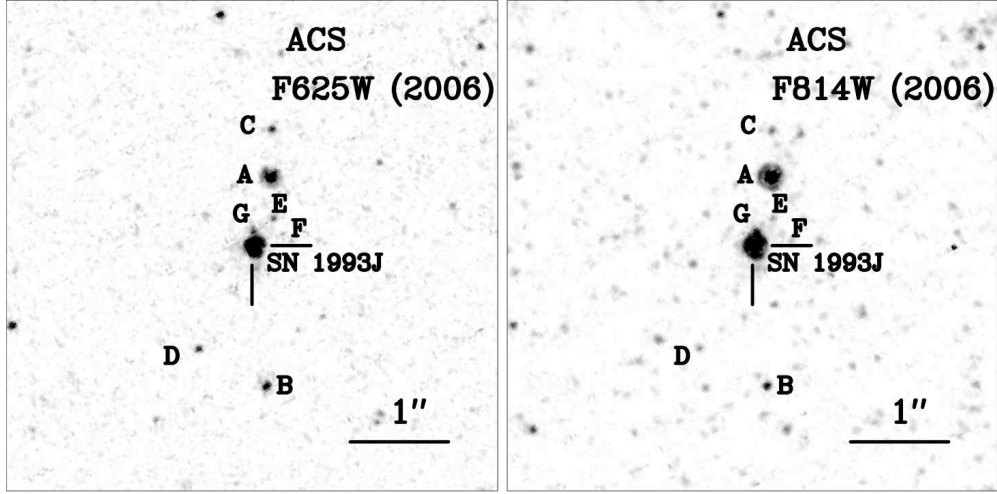


Figure S5: The site of SN 1993J. **Left)** HST ACS HRC F625W image from 03 Nov 2006. The pixel scale is 0.025'' per pixel, and the image has been rotated to have North up, East left. The stars in the vicinity of SN 1993J are labelled according to the established scheme (21, 22). **Right)** Same as for the left, except an HST ACS HRC F814W image from 01 Nov 2006.

to the appropriate Johnson  $UBV$  and Cousins  $R_cI_c$  colours (S6).

The pre-explosion photometry was corrected for the weighted contributions of stars A, B, C and D (as identified in Fig. S5), which produced the largest contribution to the excess flux (in particular in the  $U$  and  $B$  bands); while Stars E, F and G were not included in the calculation due to their faintness. Photometry of these stars in all recent HST WFPC2 and ACS observations (as listed in Tables S1 and S2) were used to determine average  $UBVRI$  magnitudes as well as assess photometric variability. This photometry is presented in Table S8. The subtraction of flux corresponding to a magnitude  $m_2$  from an object of magnitude  $m_1$  gives a new magnitude  $m'$  given by:

$$m' = -2.5 \log(f_1 - f_2) = m_1 - 2.5 \log\left(1 - \frac{1}{k}\right) \quad (2)$$

where  $k = 10^{(m_1 - m_2)/-2.5}$ .

The brightness of SN 1993J at 31 Jan 1995, 28 May 2002, 15 Jul 2004 and 1/3 Nov 2006 (as

Table S8: Photometry of Stars A, B, C and D in the vicinity of SN 1993J, the excess flux contribution and the corrected progenitor photometry.

Star	U	B	V	R	I	Distance (")
A*	23.387 (0.017)	23.808 (0.362)	22.634 (0.878)	21.523 (0.644)	20.530 (0.300)	0.74
B	23.080 (0.033)	23.088 (0.009)	22.989 (0.006)	23.042 (0.018)	22.917 (0.020)	1.43
C	23.079 (0.051)	23.708 (0.013)	23.681 (0.009)	23.742 (0.019)	23.304 (0.011)	1.21
D	22.961 (0.065)	23.704 (0.014)	23.827 (0.011)	23.907 (0.023)	23.906 (0.033)	1.19
$\sigma_x$ (")	0.85	0.61	0.69	0.77	0.53	
Excess	22.129 (0.024)	23.045 (0.124)	22.323 (0.495)	21.492 (0.450)	20.971 (0.277)	
AHR <sup>1</sup>	21.450 0.200	21.730 0.070	20.720 0.040	19.940 0.080	19.430 0.170	
AHR Corr. <sup>2</sup>	22.283 (0.431)	22.114 (0.113)	21.002 (0.155)	20.237 (0.140)	19.731 (0.241)	

\* Star A identified as variable (quoted uncertainty gives combined photometric errors and the range of variability as measured at the epochs of the observations given in Tables S1 and S2).

<sup>1</sup> Ground-based photometry of the progenitor object, including the excess flux contribution from unresolved nearby stars (17).

<sup>2</sup> Photometry of the progenitor binary system corrected for the excess flux contribution from nearby stars.

Table S9: HST WFPC2 and ACS photometry of SN 1993J at 31 Jan 1995, 28 May 2002, 15 Jul 2004 and 1/3 Nov 2006. Magnitudes are given in the standard Johnson-Cousins *UBVRI* system.

Date	U	B	V	R	I
31 Jan 1995	18.512 (0.011)	19.116 (0.006)	18.767 (0.003)	17.856 (0.002)	18.557 (0.004)
28 May 2002	21.032 (0.024)	21.195 (0.011)	20.317 (0.021)	...	...
15 Jul 2004	21.320 (0.022)	21.430 (0.042)	20.515 (0.020)	20.441 (0.020)	20.078 0.041
1/3 Nov 2006	...	21.663 (0.042)	20.683 (0.030)	20.687 (0.062)	20.232 (0.091)

presented in Fig. 2, in the main body of the paper) are given in Table S9.

The photometry presented of SN 1993J and the surrounding stars are approximately consistent with previously presented photometry of these objects (21, 26). Minor differences may have arisen due to intrinsic photometric variability (see Star A), changes in the adopted zeropoints in the intervening period between the publication of those studies and differences in the filter responses between the WFPC2 and ACS instruments. The evolution of the SN 1993J light curve, relative to the limits on the brightness of the binary progenitor system, corrected for the flux excess, is shown as Fig. S6.

## References and Notes

- S1. A. E. Dolphin, *PASP* **112**, 1383 (2000).
- S2. P. B. Stetson, *PASP* **99**, 191 (1987).
- S3. A. E. Dolphin, *PASP* **112**, 1397 (2000).

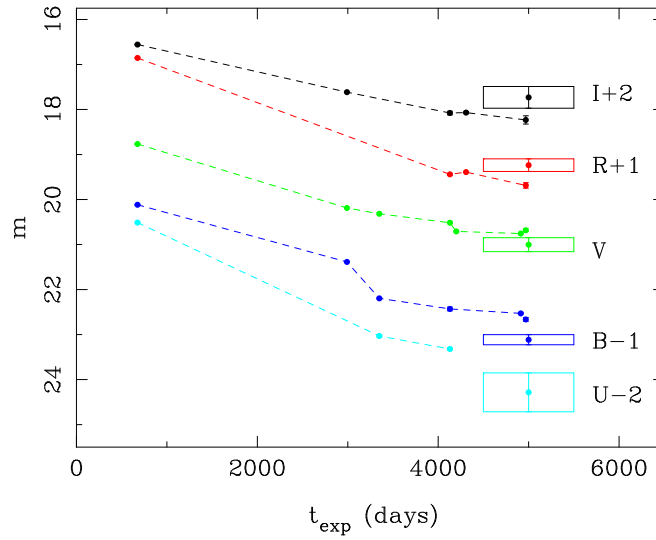


Figure S6: The late-time HST light curve of SN 1993J. The boxes show the measured brightness, corrected for excess flux, of the binary progenitor system. The photometric data is plotted in day since the date of explosion (JD 2449074; (S7)).

S4. J. A. Holtzman, J. J. Hester, S. Casertano, et al., *PASP* **107**, 156 (1995).

S5. I. Jorgensen, *ArXiv e-prints* (2008).

S6. M. Sirianni, et al., *PASP* **117**, 1049 (2005).

S7. J. R. Lewis, et al., *MNRAS* **266**, L27+ (1994).